CHAPTER 4

CHARACTERIZATION OF SEMICONDUCTOR NANOPARTICLES

4.1. **Introduction**:

Characterization and understanding of the prepared semiconductor nanostructure are an important and integral part of nanomaterials research. Since the nanostructures are too small to be visualized with conventional optical microscope, it is essential to use appropriate tools to characterize their structure in detail at the molecular or atomic level. This is important not only for understanding their fundamental properties but also for exploring their functional and technological performance in technological applications. But one of the critical challenges in nanotechnology and nanoscience field is the inability and lack of instruments to observe measure and manipulate the prepared material at nanometer level. Hence, one of the current key objectives is to adopt and develop a range of techniques that can characterize the structural, optical and morphological properties of nanostructured nanomaterials [1-3].

When the size of the material progressively reduces from microscopic dimension down to the scale of a few nanometer, there are some consequences for the atomic structure. They are firstly, interface are created in which the local atomic arrangements are different from those of the crystal lattice. As the grain size is reduced, the number of interfaces increases, and the fraction of atoms on interface sites becomes comparable to the number of crystal lattice atoms. Hence the overall properties of the solid will no longer be determined by the atomic interactions in the crystal lattice alone. Instead, the material can have novel properties reflecting the contribution from the interfaces. Secondly, the atomic structure in the interior of the crystallite is modified through the introduction of defects, strain fields or crystal lattice position. In addition, nanometer sized isolated crystallites and bulk nanocrystalline solids can differ from macroscopic crystals with respect to their crystallographic phase and their lattice constant. Many properties will reflect the combined effect of these structural changes, which is of the

reduction of length scale on which there is coherency in the atomic arrangement, of the modified crystallographic structure and of the introduction of interfaces with an atomic short range order different from the one in the crystal lattice. This leads to novel and unexpected atomic arrangement and may also have dramatic effects on other physical and chemical attributes. Because of this, understanding nanocrystalline solids requires a detailed characterization of all these aspects of their atomic structure and composition.

There are a number of powerful experimental techniques that can be used to characterize structural and optical properties of nanostructured materials. Among the various characterization techniques, X-ray diffraction (XRD) is a popular and powerful method for determining crystal structure of crystalline materials. It may also be regarded as fingerprint of material for its identification. This technique is generally employed to obtain a whole range of information about the crystallographic aspects of nanomaterials. It gives the lattice parameters, crystal structure and orientation, size of the crystallite, stress and defects of the synthesized nanoparticles. Transmission electron microscope (TEM) is also a high spatial resolution of internal structure of solids and provides access to nano-structural detail. TEM is almost exclusively used in the investigation of average particle size, particle shape and particle size distribution of nanostructured material [4]. A modern TEM has the capability to directly image atoms in crystalline specimens at resolutions close to 0.1 nm, smaller than ~ 0.3 nm, allowing quantitative chemical analysis from a single nanocrystal. This type of analysis is extremely important for characterizing materials at a length scale from atoms to hundreds of nanometers. High magnification imaging with lattice contrast allows imaging of individual crystallite morphologies [5].

Scanning electron microscope (SEM) is another type of electron microscope used to extract quantitative and qualitative information pertaining to agglomerate size/shape, particle morphology and surface appearance of nanostructured materials. The composition of various elements in the prepared nanostructures can also be studied using Energy dispersive X-ray (EDX or EDS) analysis.

Semiconductor nanoparticles or nanomaterials have rich optical properties that strongly depend on size, especially when the particle size is less than the exciton Bohr radius of the material. Thus, nanomaterials especially those belonging to II – VI groups of the periodic table eg. CdS and ZnS exhibit considerable quantum size effects leading to size dependent optical and optoelectronic properties [6-8]. The fact that the band gap of these materials varies with the crystallite size makes them an interesting category of materials for potential optoelectronics application. Because of their unique optical and optoelectronic properties, nanocrystals are likely to play a key role in the emerging new fields of applications ranging from lasers [9] and optoelectronic devices [10] to biological fluorescence marking [11]. The preferred characterization methods to analyze the size dependent optical properties of nanoparticles are UV-vis absorption spectra and photoluminescence. UV-vis absorption is a very fast characterization method for the nanoparticles because the absorption features give information about the nanoparticle formation, the band gap and the size distribution of the nanoparticles. However, it is an indirect method for determining the particle size. The band gap of the particles can be calculated from the excitonic peak position which is used to determine the particle size with the help of theoretical model such as EMA (effective mass approximation method). Photoluminescence spectra provide powerful and non-destructive emission technique and can reveal the band structure and carrier transport behaviours in a material. Moreover, the doping type band gap, composition, etc. of the bulk materials or the size, path of the carrier transport etc. of the nanostructured materials can also be observed through PL spectrum. Therefore, PL can be regarded as a key technology of characterization of excitonic structure, impurity levels and structural properties of II – VI semiconductor nanoparticle [12, 13].

Fourier transform infrared (FTIR) spectroscopy is also another optical characterization technique widely used in nanostructured material. It has the advantages of high spectra resolution, good signal to noise and the ability to measure a broad region of the spectrum in a short amount of time. An infrared spectrum represents a fingerprint

of a sample with absorption peaks which correspond to the frequencies of vibration between the bonds of the atoms making up the material. Because each different material is a unique combination of atoms, no two compounds produce the exact same infrared absorption spectrum. Therefore, infrared spectroscopy can result in a positive identification.

In this chapter, the theory of the above different characterization techniques has been summarized, so also the experimental set up and layout of the experimental method used for characterization.

4.2. **X-ray Diffraction (XRD)**:

The structural characterization of the prepared samples is carried out by using PAnalytical X-ray diffractometer (XRD). The operating voltage of X-ray tube in case of X'Pert Pro was 40 kV – 30 mA. The final diffraction pattern of the data is analyzed by both X'Pert graphics software and origin graphic software (8.0 professional).

Bragg's law is the basis of X-ray diffraction (XRD). With this law, it is possible to make accurate quantification of experimental results in the determination of phase identification, crystal structure, lattice parameter of the crystalline solids. The law was derived by English Physicist Sir W.H. Bragg and his son Sir W.L. Bragg in 1913. It has been used to explain why the cleavage faces of crystals appear to reflect X-ray beams at certain angles of incidence. A typical X-ray diffractometer consists of four main components such as X-ray source, a sample holder, receiving optics and X-ray detector as shown in figure 4.1. The source and detector with its associated optics lie on the circumference of focussing circle and sample holder at the centre of the circle. The angle between the plane of the specimen and the X-ray source is θ, known as Bragg's angle and the angle between the projection of X-ray and the detector is 2θ.

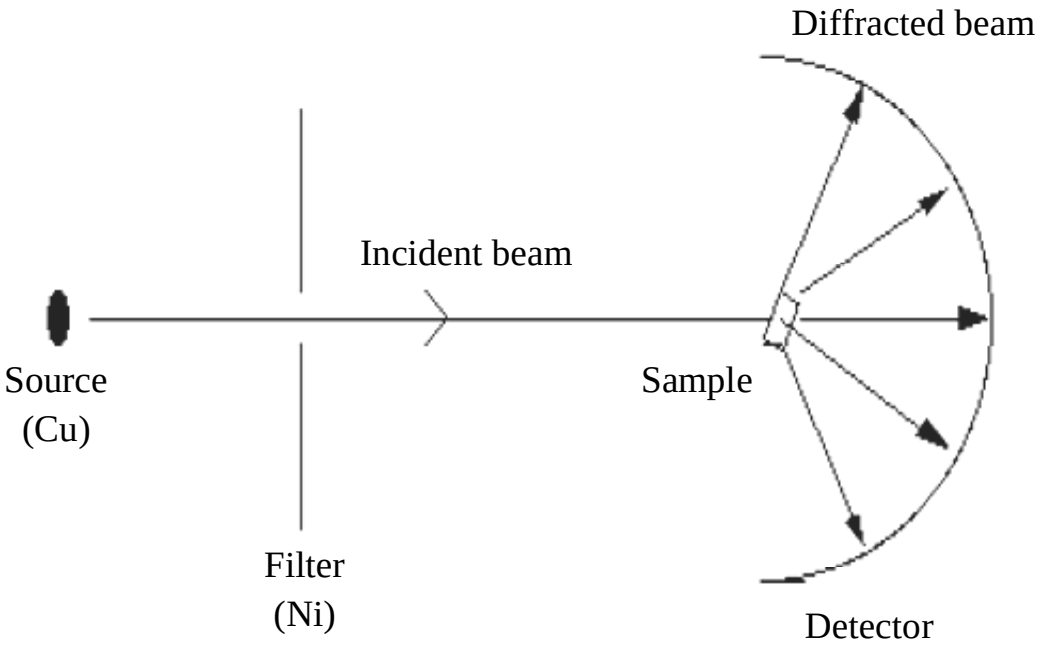

Figure 4.1: Schematic diagram of X-ray powder diffraction

For the XRD analysis, fine powder samples are mounted on the sample holder and the powder is assumed to consist of randomly oriented crystallites. When a beam of X-ray is incident upon the atoms in a crystal lattice, each atom acts as a source of scattering. The crystal lattice acts as series of parallel reflecting planes. The intensity of the reflected beam at certain angles will be maximum when the path difference between two reflected waves from two different planes is an integral multiple of λ. This condition is known as Bragg's law [14] and is given by the relation

$$2d_{hkl}\sin\theta = n\lambda \qquad \ldots\ldots\ldots\ldots\ldots\ldots\ldots\ldots\ldots\ldots \quad (4.1)$$

when n=1, 2, 3, ……. is an integer (order of diffraction usually has the value of n=1). λ is the wavelength of the X-ray, θ is the angle of the X-ray beam made with respect to plane and 'd' is the interplaner spacing between consecutive parallel planes (Figure 4.2)

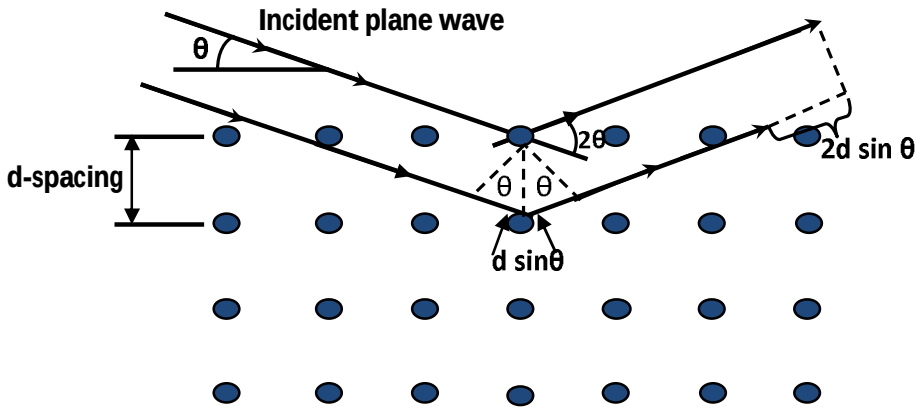

Figure 4.2: Schematic diagram for deriving Bragg's law

After recording the X-ray diffraction pattern, the first step involved is the indexing of XRD peaks. Indexing means assigning the correct miller indices to each peak of the diffraction pattern. The correct indexing is done only when all the peaks in the diffraction pattern are counted for process. There are three main methods for indexing a diffraction pattern. The main method is by comparing the measured XRD pattern with the standard powder diffraction files published by the International centre for diffraction data (ICDD).

From the X-ray diffraction study, the information about crystal structure and orientation, crystallite size, crystal planes, strain and defects of the synthesized sample can be studied [15-18].

4.2.1. **Determination of Crystallite Size**:

In the case of fine powder and with reduction in the size of the particles, the XRD pattern get broadened which indicates clearly that the particle size has been reduced. The average crystallite size of the synthesized samples can be estimated with the help of Debye Scherrer equation [19].

$$D = \frac{K\lambda}{\beta cos\theta} \qquad .2)$$

where D is the average crystallite size, K is the proportionality constant which is taken to be 0.94, λ is the wavelength of the X-ray used, β is the full width at half of the maximum intensity in radians and θ is the angle of diffraction.

4.2.2. **Determination of Lattice Constant**:

The interplanar spacing 'd' of a set of crystal planes is dependent on lattice parameters and miller indices ($h\ k\ l$) of the planes. The lattice parameter 'a' for the cubic system for each plane ($h\ k\ l$) can be evaluated from the relation [20].

$$d_{hkl} = \frac{a}{(h^2+k^2+l^2)^{1/2}}$$

$$\Rightarrow a_{cal} = d_{hkl}(h^2 + k^2 + l^2)^{1/2} \quad \ldots\ldots\ldots\ldots\ldots\ldots \quad (4.3)$$

From the Bragg's law (4.1), we get

$$2d_{hkl}sin\theta = n\lambda$$

$$\Rightarrow \quad sin\,\theta = \frac{n\lambda}{2d_{hkl}}$$

$$\Rightarrow \quad sin^2\theta = \frac{\lambda^2}{4d_{hkl}^2}$$

$$\Rightarrow \quad sin^2\theta = \frac{\lambda^2(h^2+k^2+l^2)}{4a^2}$$

$$\Rightarrow \quad sin^2\theta = \frac{\lambda^2 N}{4a^2} \quad \ldots\ldots\ldots\ldots\ldots\ldots\ldots\ldots\ldots\ldots \quad (4.4)$$

where $N = h^2+k^2+l^2$ is a number depending on ($h\ k\ l$) values. Observing the distribution of N value, the type of cubic lattice can be determined.

For hexagonal crystal, the lattice constants 'a' and 'c' can be evaluated from the relation [21]

$$\frac{1}{d_{hkl}^2} = \frac{4}{3}\left(\frac{h^2+hk+k^2}{a^2}\right) + \frac{l^2}{c^2} \quad \ldots\ldots\ldots\ldots\ldots\ldots \quad (4.5)$$

Since from Bragg's law (4.1), we get

$$2d_{hkl} sin\,\theta = n\lambda$$

$$\Rightarrow \quad sin^2\theta = \frac{\lambda^2}{4d_{hkl}^2}$$

$$\Rightarrow \quad sin^2\theta = \frac{\lambda^2}{3a^2}(h^2 + hk + k^2) + \frac{\lambda^2}{4c^2}l^2 \quad \ldots\ldots\ldots (4.6)$$

According to Vigards law, the lattice parameters for hexagonal unit cells are nearly related to cubic lattice parameters by [22]

$$a_{hex} = \left(\frac{1}{2}\right)^{1/2} a_{cubic} \text{ and } c_{hex} = \left(\frac{4}{3}\right)^{1/2} a_{cubic} \quad \ldots\ldots\ldots (4.7)$$

Therefore for ideal Wurtzite lattice, the relation between the lattice parameter is

$$c_{hex} = (1.633)a_{hex} \quad \ldots\ldots\ldots\ldots\ldots\ldots (4.8)$$

The lattice constants evaluated from highest angle reflection data are reliable but are found to be slightly different for different orientations of the sample. This is due to the divergence of the X-ray beams, refraction and absorption of X-rays by the sample etc. which involve a number of systematic errors in the measurement of θ and hence d values. So, accuracy in the determination of lattice constant is dependent upon the accuracy in the measurement of d. Since from Bragg's law (for first order diffraction $n = 1$)

$$2d\,sin\,\theta = \lambda$$

$$\Rightarrow \quad d = \frac{\lambda}{2}\,cosec\,\theta$$

$$\Rightarrow \quad \delta d = -\frac{\lambda}{2}(cosec\,\theta.cot\theta)\delta\theta$$

for $\theta = \frac{\pi}{2} = 90^o$, we have

$$\frac{\delta d}{d} = 0$$

Therefore, corrected value of lattice constant is estimated from the intercept of the Nelson-Riley plots which is a graph of the calculated values of lattice constant for different planes versus error function given by

$$f(\theta) = \frac{1}{2}\left(\frac{cos^2\theta}{sin\,\theta} + \frac{cos^2\theta}{\theta}\right) \quad \ldots\ldots\ldots\ldots\ldots \quad (4.9)$$

The intercept of this plot with x-axis gives the corrected value of lattice constant. Therefore, the values obtained from N-R plots are more or less free from systematic error.

4.2.3. **Determination of Average Strain**:

The lattice strain is developed in the synthesized samples due to some factors like doping concentration, temperature and change of state from bulk to nanocrystalline. Thus, the origin of strain is related to lattice 'mis-fit' which in turn depends upon the growth condition. The microstrain ε_{hkl} developed in the synthesized sample has been calculated by using the relation [23].

$$\varepsilon_{hkl} = \frac{\beta cos\theta}{4} \quad \ldots\ldots\ldots\ldots\ldots\ldots\ldots\ldots\ldots \quad (4.10)$$

Using this relation, magnitude of lattice strain (ε_{hkl}) along the most preferred orientation is calculated for PVA capped CdS and ZnS nanoparticles doped with different concentration of Mn^{2+}.

4.2.4. **Determination of Dislocation Density**:

Dislocations are an imperfection in a crystal associated with the misregistry of the lattice in one part of the crystal with respect to another part. Unlike vacancies and interstitial atoms, dislocations are not equilibrium imperfections, that is thermodynamic considerations are insufficient to account for their existence in the observed densities. In fact, the growth mechanism involving dislocation is a matter of importance [17].

$$\delta = \frac{n}{D^2} \quad \ldots\ldots\ldots\ldots\ldots\ldots\ldots\ldots \quad (4.11)$$

where '*D*' is the crystallite size obtained from XRD data and '*n*' is a factor which is equal to unity giving minimum dislocation density.

4.3. **Transmission Electron Microscope (TEM)**:

Transmission electron microscopy (TEM) is a microscopy technique whereby a beam of electrons is transmitted through a very thin sample and interact with the sample as it passes through. The interaction of the electrons transmitted through the sample form an image. This image is magnified and then focussed onto a fluorescent screen or it can be detected by a CCD (Charge Coupled Device) camera. The first practical TEM was built by Albert Prebus and James Hillier at the University of Toronto in 1938 using the concepts developed earlier by Max Knoll and Ernst Ruska. It is unique because it can provide a real space image on the atomic distribution in the nanocrystals and on its surface [3].

The imaging capability of TEM has a significantly higher resolution than that of light microscopes because of the small de Broglie wavelength of electrons. The instrument is therefore enabled to examine fine detail even as small as a single layer of atoms. TEM is used in a range of scientific fields as a major analysis method in both biological and physical sciences. Applications of TEM are in material science, pollution and semiconductor research, virology and cancer research [24].

The operation of the TEM requires electrons that are generated by a process known as thermionic discharge in the same manner as the cathode in the cathode ray tube. The electrons are accelerated by an electric field then it is focussed and magnified by a set of magnetic lenses. Figure 4.3 shows the block diagram of TEM. The image that is formed is either shown on a fluorescent screen or on a monitor and is printed on photographic film. The resolution power is usually restrained by the technique with which the preparation is achieved and quality of the lens system. Current Transmission

electron microscopes offer resolution up to 0.1 nm at 300 KV and probe diameter up to 0.39 nm.

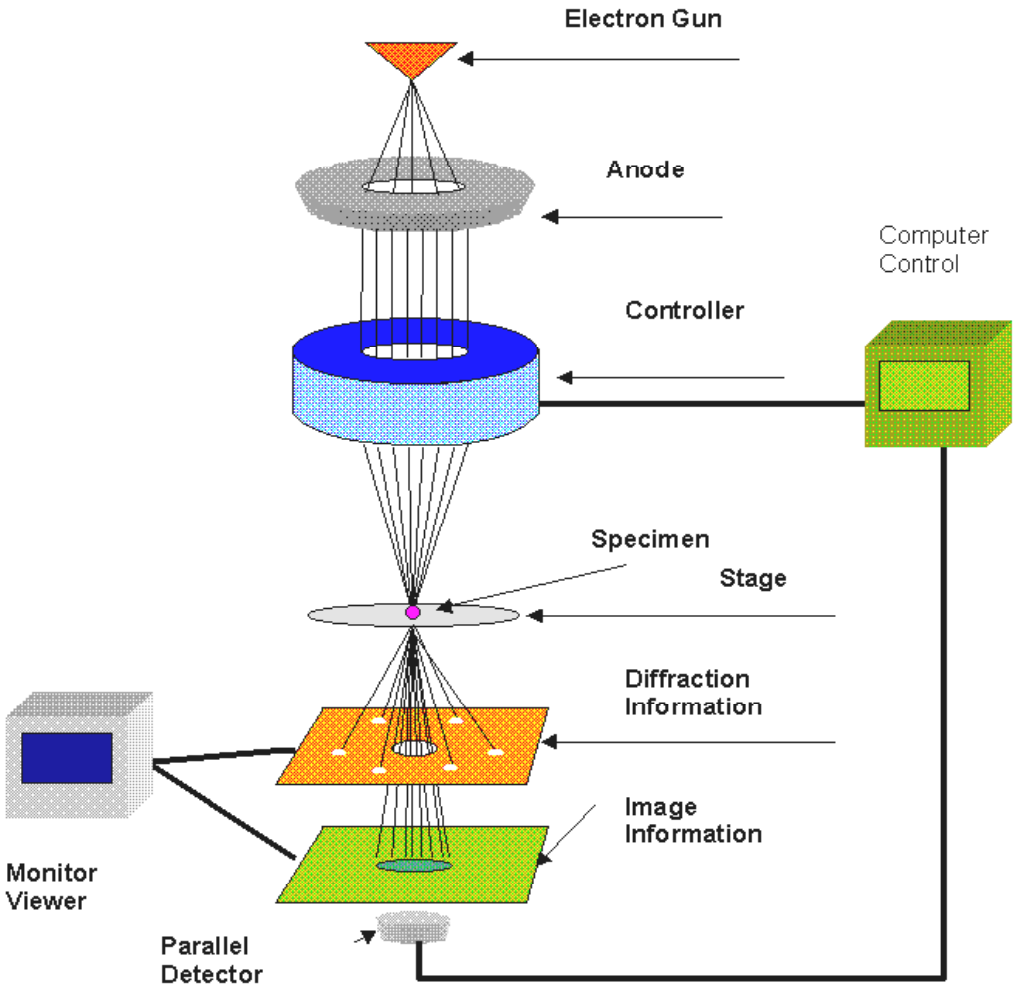

Figure 4.3: Block diagram of Transmission Electron Microscope (TEM)

TEM exploits three different interactions of electron beam - specimen, unscattered electrons (transmitted beam), elastically scattered electrons (diffracted beam) and inelastically scattered electrons. Different types of imaging are obtained in TEM, using the aperture property as well as the different types of electrons. Diffraction patterns are shown because of the scattered electrons. If the unscattered beam is selected, we

obtain the Bright Field (BF) image and if diffraction beam is selected by the objective aperture we obtain the Dark Field (DF) image [25, 26].

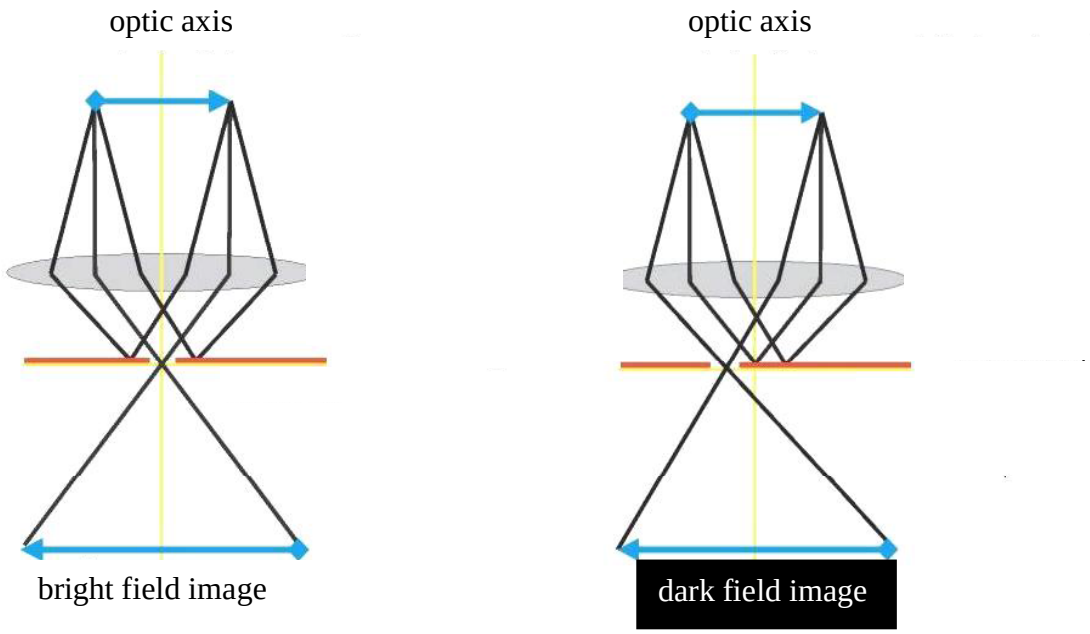

Figure 4.4: Bright field imaging and dark field imaging

The DF image is formed by effectively cutting out all the diffracted beams, leaving out only transmitted beam to form the image. The bright field image is bright only in areas that have crystalline planes that are tilted such that they do not satisfy the Bragg condition. The DF image will be obtained on the other hand if the transmitted beams are blocked instead of diffracted beams.

4.3.1. **High Resolution Transmission Electron Microscope (HRTEM)**:

High resolution transmission electron microscope (HRTEM) can generate lattice images of the crystalline material allowing the direct characterization of the samples atomic structure [27]. The resolution of the HRTEM is 1 nm or small. However, the most difficult aspect of the TEM technique is the preparation of samples. HRTEM is made possible by using a large diameter objective diaphragm that admits not only the transmitted beam but at least one diffracted beam as well. All of the beams passed by the

objective aperture are then made to recombine in the image forming process, in such a way that their amplitude and phases are preserved. When viewed at high magnification, it is possible to see contrast in the image in the form of periodic fringes. These fringes represent direct resolution of the Bragg diffracting planes, the contrast is referred to as phase contrast. The fringes that are visible in the high resolution image originates from those planes that are oriented as Bragg reflecting planes and that possess interplaner spacings greater than the lateral spatial resolution limits of the instrument.

4.3.2. **Selected Area Electron Diffraction Pattern (SAED)**:

Selected area electron diffraction offers a unique capability to determine the crystal structure of individual nanomaterials and the crystal structure of the different parts of a sample. A small area of the specimen can be selected from a high resolution transmission image and its electron diffraction pattern (rings) produced on the screen of the microscope by making appropriate arrangement in the lenses of TEM. This is an optional arrangement in HRTEM. The SAED allows the researcher to determine lattice constant of the crystalline material which can help in species identification. Basically diffraction patterns are distinguishable as ring patterns resulting from single crystal diffraction or ring patterns are obtained from the randomly oriented crystal aggregates. For nanocrystalline structure, the diffraction patterns will be a diffused ring patterns.

The *d* spacing of the planes corresponding to the rings can be determined by the following relation

$$Dd = L\lambda \qquad \text{..... (4.12)}$$

where '*L*' is the effective camera length, λ is the de Broglie wavelength of the accelerating electrons. '*D*' is the ring diameter of a standard electron diffraction pattern and '*d*' is the interplanar spacing [28]. The term in the right hand side of the above equation is known as the camera constant.

4.4. **Scanning Electron Microscope (SEM)**:

Surface morphology is an important characterization technique while studying nanostructure material. Scanning electron microscope (SEM) is an important characterization tool used to study the surface morphology of the prepared nanostructured material. SEM is a type of electron microscope that images the sample surface by scanning it with a high energy beam of electron in a raster scan pattern. SEM uses a focussed beam of high-energy electrons to generate a variety of signals at the surface of solid specimens. The signals that derive from electron sample interaction reveal information about the sample including external morphology. Chemical composition, crystalline structure and orientation of materials make up the samples [29]. Figure 4.5 shows the schematic diagram of Scanning electron microscope.

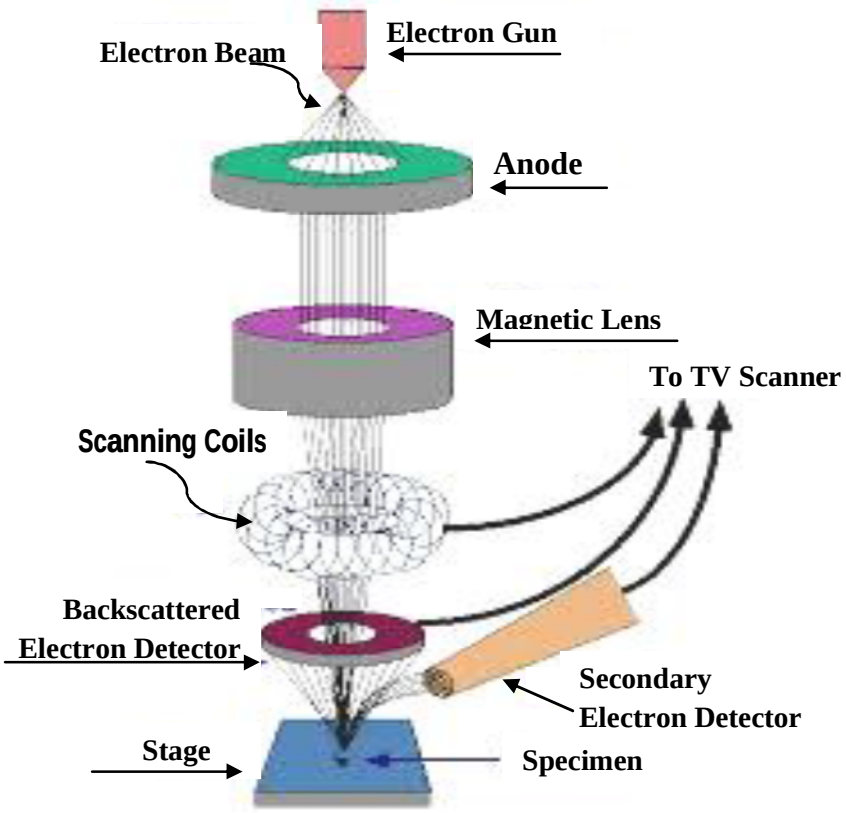

Figure 4.5: Schematic Diagram of Scanning Electron Microscope (SEM)

The SEM is an instrument that produces a largely magnified image by using electrons instead of light to form an image. A beam of electron is produced at the top of the microscope by an electron gun. The electron beam follows a vertical path through the microscope, which is held within a vacuum. The electron beam travels through electromagnetic fields and lenses which focus the beam down towards the sample. Once the beam hits the sample, electrons and X-rays are ejected from the sample.

Electrons are emitted via field emission from a tungsten cathode and are accelerated towards the anode. Tungsten is used because it has the highest melting point and lowest vapour pressure of all metals thereby allowing it to be used for electron emission. When the primary electron beam interacts with the sample, the electron lose energy by repeated scattering and absorption within a teardrop shaped volume of the specimen known as the interaction volume which extends from less than 500 nm to around 5 μm into the surface. The size of the interaction volume depends on the beam accelerating voltage, the atomic number of the specimen and specimen's density. An image is formed by collecting the emission of electron scattered both elastically and inelastically from the specimen. However, the SEM imaging of a non-conductive sample is plagued with so called charging effect. In the non-conductive sample, the electrons are accumulated and the incoming electrons are repelled by the charge surface. Practically a thin layer of Au (gold) or carbon will be coated prior to the SEM imaging for non-conductive sample in order to avoid the charging effect.

4.4.1. **Energy Dispersive X-ray (EDX) Analysis**:

The chemical composition of the synthesized powder was studied using energy dispersive X-ray (EDX) analysis. It is also sometimes referred to as EDAX or EDS. The EDX analysis works as an integrated feature of Scanning electron microscope (SEM) and cannot be operated on its own without the later [30, 31]. During EDX analysis, the sample is bombarded with an electron beam inside the SEM. The bombarding electrons collide with the specimen atom's own electrons knocking some of them in the process. A position vacated by an ejected inner shell electron is eventually occupied by a higher

energy electron from an outer shell. To be able to do so, however, the transferring outer electron must give up some of its energy by emitting an X-ray. The amount of energy released by the transferring electron depends on which shell it is transferring to. Furthermore, the atom of every element releases X-rays with unique amounts of energy during the transferring process. Thus, by measuring the energy of the X-rays emitted by a specimen during electron beam bombardment, the identity of the atom from which the X-ray was emitted can be established. The output of an EDX analysis is an EDX spectrum which is a plot of how frequently X-ray is received for each energy level.

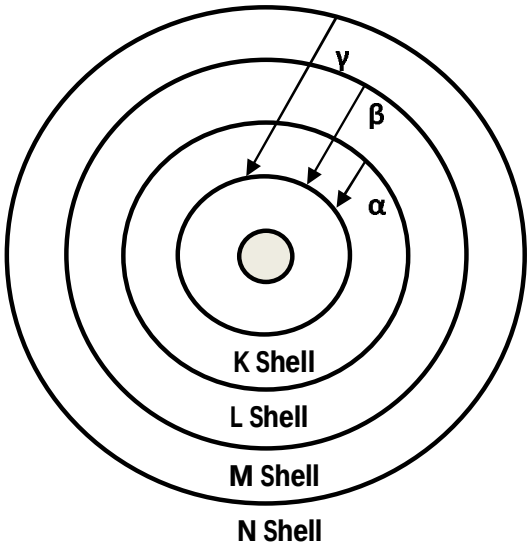

Figure 4.6: Probability shells around the nucleus

EDX spectrum normally displays peaks corresponding to the energy levels for which the most X-rays had been received. Each of these peaks is unique to an atom and therefore corresponds to a single element. The higher peak in a spectrum, the more concentrated the element is in the sample. An EDX spectrum plot not only identifies the element corresponding to each of the peaks but the type of X-ray to which it corresponds as well.

4.5. **UV-vis Spectrophotometer**:

Ultraviolet-visible spectrophotometer or ultraviolet-visible spectroscopy involves the spectroscopy of photons in the UV-visible region. This means it uses light in the visible and adjacent near ultraviolet (UV) and near infrared (NIR) ranges. The absorption in the visible ranges directly affects the colour of the chemicals involved. In this region of the electromagnetic spectrum, molecules undergo electronic transitions. This technique is complementary to fluorescence spectroscopy. Fluorescence deals with transitions from the excited state to the ground state, while absorption measures transitions from the ground state to the excited state. Thus, when an electron from the ground state (valence band) absorbs some energy, the electrons are excited and jump to the excited state (conduction band). The excitation energy should be greater than or equal to the band gap of the material. Band gap is the energy difference between conduction band and valence band. For the excitation less than the band gap, energy is transmitted and hence the band gap of the semiconductor nanomaterials can be determined from optical absorption/transmission spectra. The optical absorbance/transmittance studies are carried out using Perkin-Elmer UV-visible spectrophotometer.

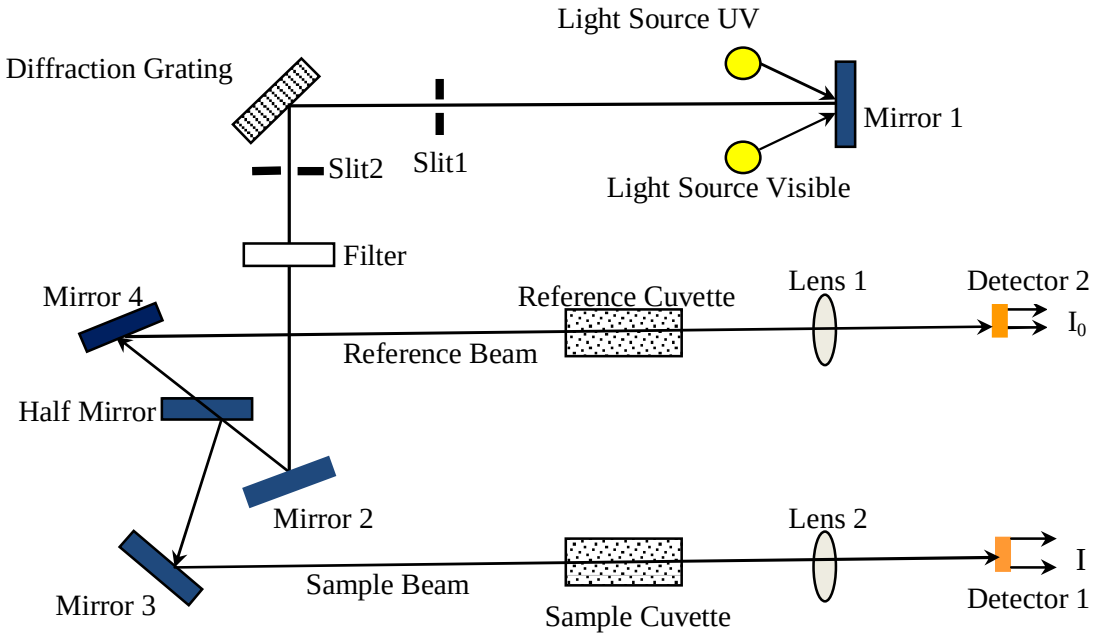

Figure 4.7: Schematic diagram of UV-visible spectrophotometer (double beam)

Figure 4.7 shows the schematic diagram of the UV-visible spectrophotometer. A beam of light from a visible/UV light source is separated into its component wavelengths by a prism or diffraction grating. Each monochromatic (single wavelength) beam in turn split into two equal intensity beams by a half silvered mirror. One beam denoted as the sample beam passes through the sample which we want to observe the absorption and another beam (Reference beam) has passed through a reference sample. The intensity of the reference beam which should have suffered little or no light absorption is defined as I_0. The intensity of the sample beam is defined as I. Over a short period of time, the spectrometer automatically scans all the component wavelengths. The ultraviolet (UV) region scanned is normally 200 nm to 400 nm and visible portion is from 400 nm to 800 nm. If the sample compound does not absorb light of a given wavelength, then $I = I_0$. However, if the sample compound absorb light, then I is less than I_0 and this difference may be plotted on a graph versus wavelength, then absorbance is given by

$$A\ (absorbance) = \frac{log\ I_0}{I} \qquad \ldots\ldots\ldots\ldots\ldots\ldots\ldots\ldots \quad (4.13)$$

From the graph of the absorbance versus wavelength (λ), the value of λ should have maximum point and from the maximum point the band gap (E_g^{nano}) of the sample can be calculated by using the wave-energy equation

$$E_g^{nano} = h\nu_g^{nano} = \frac{hc}{\lambda_g^{nano}} \qquad \ldots\ldots\ldots\ldots\ldots \quad (4.14)$$

where h is the Planck's constant, c is the velocity of light, λ is the absorption wavelength and E_g^{nano} is the energy band gap of the semiconductor nanoparticle in the absorption spectra.

4.5.1. **Effective Mass Approximation (EMA)**:

The effective mass approximation (EMA) calculates the size dependence of the band gap quantum mechanically with the particle in a box approach and uses the effective masses of electron and hole in the term for the kinetic energy which leads to the following result [32]. EMA models a single particle Hamiltonian with the dispersion

relation of bulk bands near the minimum and maximum. The kinetic energy of the single particle Hamiltonian is described by replacing a bare electron mass with an effective mass. The effective mass *m** is obtained from the band curvature near the minimum and maximum when the dispersion relation *E(k)* of the band is given by

$$\frac{1}{m^*} = \frac{1}{\hbar^2}\frac{\partial^2 E(k)}{\partial k^2}\Big|_{k=0} \qquad \text{..... (4.15)}$$

In the simplest case where the coupling between the lowest conduction and the highest valence bands is negligible, the effective Hamiltonians of low-lying electron and hole levels in nanoparticles can be separately written as

$$H_e = -\frac{\hbar^2\nabla^2}{m_e^*} + V_e(r) + E_g$$

$$H_h = -\frac{\hbar^2\nabla^2}{m_h^*} + V_h(r)$$

where m_e^* and m_h^* are electron and hole effective masses. E_g is a bulk band gap i.e. the energy difference between the bottom of the lowest conduction band and top of the highest valence band. The confinement of the nanoparticle is imposed in the potential $V(r)$. In a spherical particle, the confining potential can be written as

$$V(r) = V_0\theta(r - R)$$

where $\theta(r - R)$ is the step function and R is the radius of the nanoparticle. The constant V_0 is determined by a band offset between the nanoparticle and the surrounding material. Calculation of this energy level based on the EMA has been proposed [33, 34]. The Schrodinger equation has been solved through variational methods. Similar results are obtained by all authors for the smallest crystallites, typically for radius lower than that of bulk exciton. In this case, they have shown that the electron and hole are practically uncorrelated and can be considered to be individual particles. In this range of sizes a good evaluation of the ground state is derived as [33, 34].

$$\Delta E_g = \frac{h^2}{8R^2}\left(\frac{1}{m_e^*} + \frac{1}{m_h^*}\right) - \frac{1.8e^2}{4\pi\varepsilon_0\varepsilon R} - \frac{0.124e^4}{8\pi^2\varepsilon_0^2\varepsilon\hbar}\left(\frac{1}{m_e^*} + \frac{1}{m_h^*}\right)^{-1} \quad \ldots\ldots\ldots\ldots (4.16)$$

where $\Delta E_g = E_g^{nano} - E_g^{bulk}$ is the band gap of the nanoparticle. m_e^* is the effective mass of electron, m_h^* is the effective mass of hole, R is the radius of the particle, ε is the dielectric constant and ε_0 is the permittivity of free space. In the above equation, the first term is the kinetic energy of both electron and hole. The second is the coulomb attraction. The last term corresponds to the correlation between the two particles. The kinetic energy is dominant but the coulomb interaction cannot be neglected.

The accuracy of the EMA has inherent limitations. This approach fails for the smallest crystallite sizes because of the oversimplified description of the crystal potential as a spherical well with an infinity high potential at the interface [32]. Another problem could be the fact that the effective masses were assumed to be constant which is only correct when dealing with electronic states near the band edges [35]. Therefore, the EMA is applicable to relatively large quantum dots with interior properties outweighing surface properties.

4.5.2. **The Tight Binding Model**:

Nanometer sized semiconductor crystallites, if treated correctly, should be described in the same way as very large molecules. That means that particular number of atoms and their spatial configuration should be regarded rather than the size.

In II - VI zinc blende crystals such as CdS and ZnS, each Cd and Zn atom is surrounded tetrahedrally by four S atoms and vice versa. With three p and one s atomic orbital on each cation and anion, we will obtain four sp^3- hybridised atomic orbitals. When these atoms assemble in a cluster, these orbitals should be treated as a set of bond rather than atomic orbitals between nearest neighbour atoms. They so form a set of bonding orbitals σ and a set of antibonding orbitals σ^* [36]. As the number of atoms in the crystallite grows, each of the localized bond orbital sets form molecular orbitals

extended over the crystallite that finally develop into conduction and valence bands. The highest occupied molecular orbital (HOMO) becomes the top of the valence band and the lowest unoccupied molecular orbital (LUMO) becomes the bottom of the conduction band. The HOMO-LUMO spacing tends to the band gap energy of the bulk nanocrystals. In Figure 4.8, it can be seen that with decreasing number of atoms in the particle the band gap increases and we obtain discrete energy levels [37].

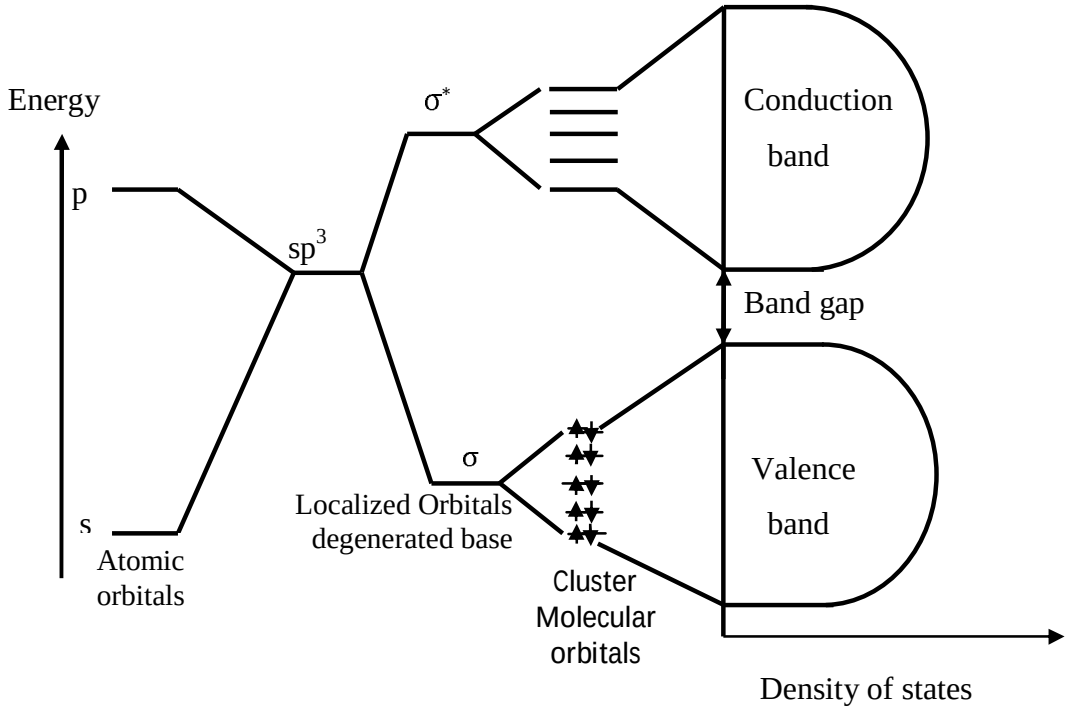

Figure 4.8: Evolution from molecular orbitals into bands

With the tight binding model the electronic structure for very small crystallites can be calculated using quantum mechanical methods [38] but it is not possible to calculate the energy levels for big clusters [32] because too many atoms have to be taken into account.

4.6. **Photoluminescence**:

Photoluminescence is a non-destructive, contactless, optical technique for probing the electron structure of materials. Photo-excitation occurs when light is directed onto a sample and it gets absorbed and imparts excess energy into the material. One of

the ways this excess energy can be dissipated by the sample is through the emissions of light. Thus, this process is known as luminescence. Hence, when the luminescence is accompanied by photo-excitation, it is known as photoluminescence (Figure 4.9). The intensity and spectral content of the photoluminescence is a direct measure of various important material properties.

Electrons within the material moving into permissible excited states are caused by photoexcitation. Excess energy is released when these electrons return to their equilibrium states and this may include the emission of light (radiative process) or a non-radiative process as shown in figure 4.9. The energy of the emitted light relates to the difference in the energy levels between the two electron states that is involved in the transition between the excited and equilibrium state. The relative contribution of the radiative process is related to the quantity of the emitted light.

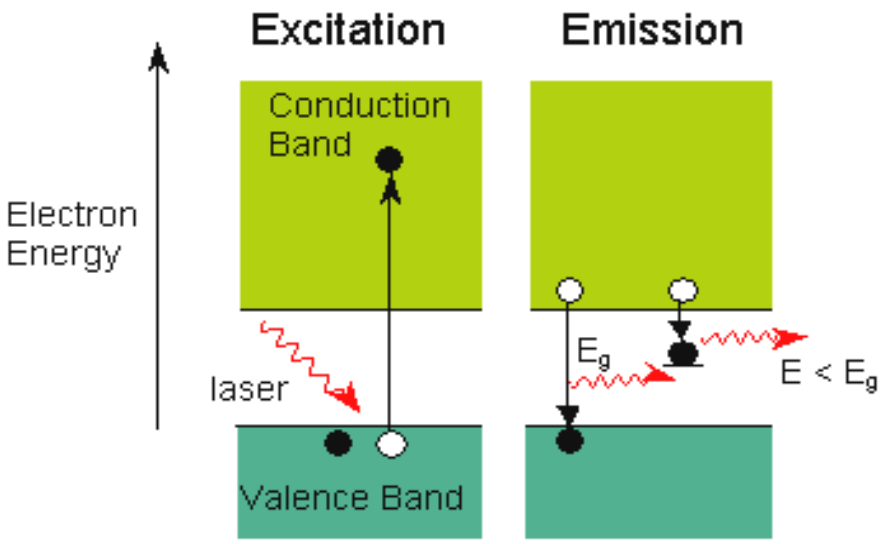

Figure 4.9: Mechanism of photoluminescence

In order to probe the band gap of the material, light of shorter wavelength (greater energy) is required to excite the material. Thus, when the sample is irradiated with a photon beam of energy $h\nu > E_g$, the absorbed photons bring electrons to the conduction band leaving behind holes in the valence band that is electron hole pairs are

produced by the optical excitation. Energy and wavelength must be conserved during this process. The electron loses some energy until it reaches the bottom of the conduction band. Two possible transitions are shown in figure 4.9. In one case, the electrons combine immediately with a hole in the valence band emitting a photon of energy E_g and in another case, the electron gets stuck in the mid-gap state emitting a lower energy photon [39].

Photoluminescence can be used in many different ways such as:

4.6.1. **Determination of the band gap**:

The most common radiative transition in semiconductors is between states in the conduction and valence bands, with the energy difference between these bands being known as the band gap. When working with new compound semiconductors the determination of the band gap is particularly useful.

4.6.2. **Detection of impurity levels and defects**:

Localized defect levels are also involved in radiative transitions in semiconductors. Specific defects can be identified by using the photoluminescence energy associated with these levels and their concentration can be determined by the amount of photoluminescence.

4.6.3. **Mechanism of recombination**:

Recombination or the return of electrons to their equilibrium states can involve both radiative and non-radiative process. The dominant recombination process directly relates to the amount of photoluminescence and its dependence on the level of photo-excitation and temperature. The understanding of the underlying physics of the recombination mechanism is greatly assisted by the analysis of the photoluminescence [40].

4.6.4. **Photoluminescence Excitation**:

The choice of excitation is critical in any PL measurement. The excitation energy and intensity will have profound effects on the PL signal. Although the excitation condition must be considered carefully, the strength of the PL technique relies heavily on the flexibility that these adjustable parameters provide. Because the absorption of most materials depends on energy, the penetration depth of the incident light will depend on the excitation wavelength. Hence, different excitation energies probe different regions of the sample. The excitation energy also selects the initial excited state in the experiment. Because lasers are monochromatic, intense and readily focussed, they are the instruments of choice for photoluminescence excitation. For many applications, the excitation energy is not critical. Here, a relatively inexpensive He-Ne or diode laser will often satisfy the basic requirement of light exceeding the band gap energy. In more demanding experiments, the laser is chosen carefully to probe a particular depth or to excite a particular species in the sample.

Unlike the excitation energy, which may or may not be important, the excitation intensity will influence the result of any PL experiment. The excitation intensity controls the density of photoexcited electrons and holes, which governs the behaviour of these carriers. Each electron hole recombination mechanism has a distinct functional dependence or carrier density. For example, the number of interface and impurity states is finite and recombination at these sites will saturate at high excitation. In addition, the photoexcited carriers themselves can alter the distribution of interface states. Thus, the excitation intensity must be calibrated accurately and controlled precisely.

4.7. **Fourier Transform Infrared (FTIR) Spectroscopy**:

Fourier transform infrared (FTIR) spectroscopy is a technique that provide information about the chemical bonding or molecular structures of materials, whether organic or inorganic chemicals. It is used to identify the unknown materials present in the specimen. The technique works on the fact that bonds and groups of bonds vibrate at

characteristic frequencies. A molecule that is exposed to infrared rays absorbs infrared energy at frequencies which are characteristic of that molecule. During FTIR analysis, a spot on the specimen is subjected to a modulated IR beam. The specimen's transmittance and reflectance of the infrared rays at different frequencies is translated into an IR absorption plot consisting of reverse peaks. The resulting FTIR spectral pattern is then analyzed and matched with known signatures of identified materials in the FTIR library. FTIR spectroscopy does not require a vacuum, since neither oxygen nor nitrogen absorbs infrared rays. FTIR analysis can be applied to minute quantities of materials whether solid, liquid or gaseous. When the library of FTIR spectral patterns does not provide an acceptable match, individual peaks in the FTIR plot may be used to yield partial information about the specimen. Figure 4.10 shows the schematic diagram of a Fourier transform infrared spectrometer.

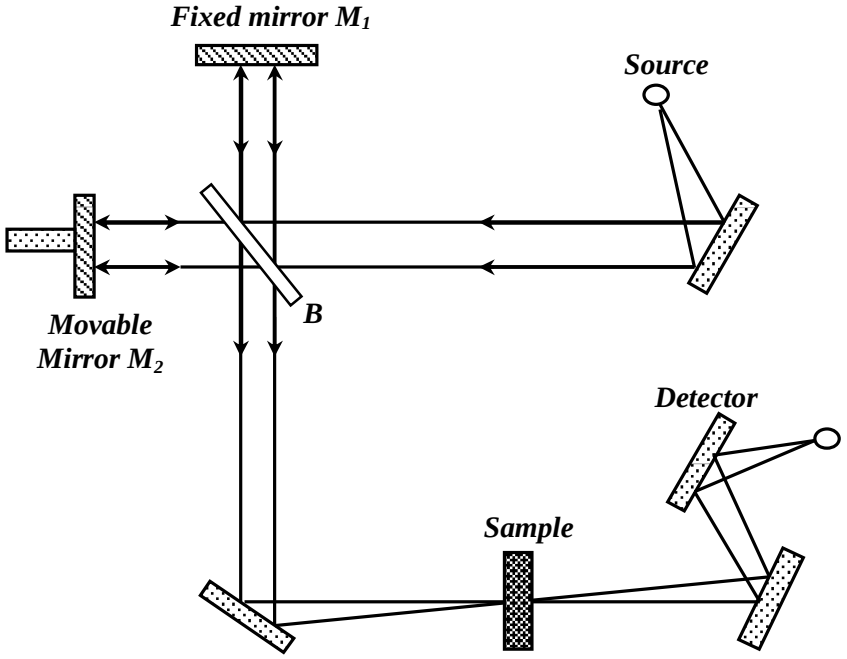

Figure 4.10: Schematic diagram of Fourier transform infrared (FTIR) spectrometer

A parallel beam of radiation is directed from the source to the interferometer, consisting of a beam splitter B and two mirrors M_1 and M_2. The beam splitter is a plate of

suitably transparent material coated so as to reflect 50% of the radiation falling on it. Thus half of the radiation goes to M_1 and half to M_2, returns from both these mirrors along the same path and is then recombined to a single beam at the beam splitter. If a monochromatic radiation is emitted by the source, the recombined beam leaving B shows constructive or destructive interference depending on the relative path lengths B to M_1 and B to M_2. As the mirror M_2 is moved smoothly towards or away from B, therefore a detector sees radiation alternating in intensity.

4.8. **References**:

1. Guozhong, Cao (2004). *Nanostructures and Nanomaterials Synthesis: Properties & Applications,* Imperial College Press, London.
2. Goswami, A. (1996). *Thin Film Fundamentals*, New Age International (P) Ltd., New Delhi.
3. Wang Zhong, Lin (ed) (2000). *Characterization of Nanophase Materials*, Wiley-VCH.
4. Xiao-Feng, Zhang; Zhang, Ze (2001). *Progress in Transmission Electron Microscopy*, Springer.
5. Bawendi, M.G.; Kortan, A.R.; Steigerwald, M.L.; Brus, L.E. (1997). *J. Chem. Phys.* **91**: 7282-7290.
6. Alivisatos, A.P. (1996). *J. Phys. Chem*. **100**: 13226-13239.
7. Yoffe, A.D. (1993). *Adv. Phys*. **42**: 173-266.
8. Kayanuma, Y. (1988). *Phys. Rev. B.* **38**: 9797-9805.
9. Kazes, M.; Lewis, D.Y.; Ebenstein, Y.; Mokari, T., Banin, U. (2002). *Adv. Mater.* **14**: 317-321.
10. Daboussi, B.O.; Bawendi, M.G.; Onitsuka, O.; Rubner, M.F (1995). *Appl. Phys. Lett*. **66:** 1316-1318.
11. Mitchell, G.P.; Mirkin, C.A.; Letsinger, R.L. (1999). *J. Am. Chem. Soc*. **121:** 8122-8123.
12. Kreibig, U.; Vollmer, M. (1994). *Optical properties of Metal Clusters*, Springer-Verlag, Berlin.
13. Klar, T.; Perner, M.; Grosse, S.; Von Plessen, G.; Spirkl, W.; Feldmann, J. (1998), *Phys. Rev. Lett.* **80:** 4249-4252.

14. Bragg, W.L. (1913). *Proc. Cambridge Phil. Soc.* **17**: 43-57.

15. Kalita, P.K.; Sarma, B.K.; Das, H.L. (2000). *Bull. Mater Sci*. **23**: 313-317.

16. De, C.K.; Mishra, N.K.; Ghosh, T.B. (1993). *Ind. J. Phys.* A **69**: 261-266.

17. De, C.K.; Mishra, N.K. (1997). *Ind. J. Phys*. A **71:** 530-535.

18. Chaliha, S.; Borah, M.N.; Sarmah, P.C.; Rahaman, A. (2008). *J. optoelectron. Adv. Mater*. **10(2):** 427-433.

19. Cullity, B.D.; Stock, S.R. (2001). *Elements of X-ray diffraction*, Prentice Hall, New Jersey, 3rd edition.

20. Klug, H.P.; Alexander, L.E. (1954). *X-ray Diffraction Procedures*, John Willey and Sons Inc. New York, 2nd edition.

21. Cullity, B.D. (1978). *Elements of X-ray Diffraction* (2nd eds), Addision-Wesley Publishing Company Inc. London, 2nd edition: 327-335.

22. Roth, W.L.; Aven, M.; Prener, J.S. (edited) (1967). *Physics and Chemistry II-VI compounds*, North-Holland Publishing Company, Amsterdam. 127.

23. Sen, S.; Halder, S.K.; Sen Gupta, S.P. (1975). *Jour. Phys. Soc*. Japan. **38(6):** 1643-1645.

24. TEM, Hyperlink; http://www.wikipedia.com

25. TEM, Hyperlink; http://www.microscopy.etz.ch/TEM_BF.htm

26. TEM, Hyperlink; http://www.microscopy.etz.ch/TEM_DF.htm

27. Subramanian, A.; Marks, L.D. (2004). *Ultramicroscopy*. **98**: 151-157.

28. Flewitt, P.E.J.; Wild, R.K. (2003). *Physical methods for materials characterization*, IOP Publishing Ltd.

29. Matsuyama, H.; Koike, K. (1991). *Rev. Sci. Instrum.* **62**: 970-981.

30. Flewitt, P.E.J.; Wild, R.K. (2003). *Physical method for materials characterization*, IOP Publishing Ltd.

31. Schroder, D.K. (1998). *Semiconductor material and device characterization*, Wiley Interscience, New York.

32. Lippens, P.E., Lannoo, M. (1989). *Phys. Rev. B.* **39**: 10935-10942.

33. Kayanuma, Y. (1988). *Phys. Rev. B.* **38:** 9797-9805.

34. Wang, Y.; Herron, N. (1991). *J. Phys. Chem*. **95**: 525-532.

35. Henglein, A. (1989). *Chem. Rev*. **89**: 1861-1873.

36. Bawendi, M.G.; Steigerwald, M.L.; Brus, L.E. (1990). *Annu. Rev. Phys. Chem*. **41**: 477-496.

37. Wang, Y.; Suna, A.; Mahler, W.; Kasowski, R. (1987). *J. Chem. Phys*. **87:** 7315-7322.

38. Gaponenko, S.V. (1998). *Optical properties of Semiconductor Nanocrystals*, New York, Cambridge University Press.

39. Hanzawa, H.; Kobayashi, M.; Matsuda, O.; Murase, K.; Giriat, W. (1999). *Phys. Status Solidi(a)*. **175**: 715-724.

40. Ntwaeborwa, OM; Swart, HC; Kroon, RE; Botha, JR; Ngaruiya, JM; Holloway, PH (2008). *Photoluminescence Research Progress.* 287-306.